



UNIVERSITY OF LEEDS

This is a repository copy of *Systematic Review of Synthetic Computed Tomography Generation Methodologies for Use in Magnetic Resonance Imaging–Only Radiation Therapy*.

White Rose Research Online URL for this paper:  
<http://eprints.whiterose.ac.uk/121200/>

Version: Accepted Version

---

**Article:**

Johnstone, E, Wyatt, JJ, Henry, AM [orcid.org/0000-0002-5379-6618](http://orcid.org/0000-0002-5379-6618) et al. (6 more authors) (2018) Systematic Review of Synthetic Computed Tomography Generation Methodologies for Use in Magnetic Resonance Imaging–Only Radiation Therapy. *International Journal of Radiation Oncology - Biology - Physics*, 100 (1). pp. 199-217. ISSN 0360-3016

<https://doi.org/10.1016/j.ijrobp.2017.08.043>

---

© 2017 Elsevier Inc. This manuscript version is made available under the CC-BY-NC-ND 4.0 license <http://creativecommons.org/licenses/by-nc-nd/4.0/>

**Reuse**

This article is distributed under the terms of the Creative Commons Attribution-NonCommercial-NoDerivs (CC BY-NC-ND) licence. This licence only allows you to download this work and share it with others as long as you credit the authors, but you can't change the article in any way or use it commercially. More information and the full terms of the licence here: <https://creativecommons.org/licenses/>

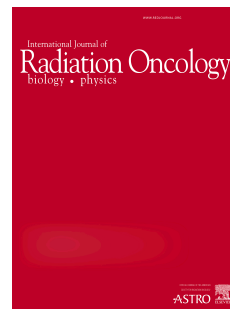
**Takedown**

If you consider content in White Rose Research Online to be in breach of UK law, please notify us by emailing [eprints@whiterose.ac.uk](mailto:eprints@whiterose.ac.uk) including the URL of the record and the reason for the withdrawal request.



[eprints@whiterose.ac.uk](mailto:eprints@whiterose.ac.uk)  
<https://eprints.whiterose.ac.uk/>

# Accepted Manuscript



A systematic review of synthetic CT generation methodologies for use in MRI-only radiotherapy

Emily Johnstone, MSc, Jonathan J. Wyatt, MSc, Ann M. Henry, MD, Susan C. Short, MBBS, PhD, David Sebag-Montefiore, FRCR, Louise Murray, PhD, Charles G. Kelly, FRCR, Hazel M. McCallum, PhD, Richard Speight, PhD

PII: S0360-3016(17)33840-3

DOI: [10.1016/j.ijrobp.2017.08.043](https://doi.org/10.1016/j.ijrobp.2017.08.043)

Reference: ROB 24489

To appear in: *International Journal of Radiation Oncology • Biology • Physics*

Received Date: 24 January 2017

Revised Date: 7 July 2017

Accepted Date: 30 August 2017

Please cite this article as: Johnstone E, Wyatt JJ, Henry AM, Short SC, Sebag-Montefiore D, Murray L, Kelly CG, McCallum HM, Speight R, A systematic review of synthetic CT generation methodologies for use in MRI-only radiotherapy, *International Journal of Radiation Oncology • Biology • Physics* (2017), doi: 10.1016/j.ijrobp.2017.08.043.

This is a PDF file of an unedited manuscript that has been accepted for publication. As a service to our customers we are providing this early version of the manuscript. The manuscript will undergo copyediting, typesetting, and review of the resulting proof before it is published in its final form. Please note that during the production process errors may be discovered which could affect the content, and all legal disclaimers that apply to the journal pertain.

# A systematic review of synthetic CT generation methodologies for use in MRI-only radiotherapy

*sCT generation methods for MRI-only RT*

Emily Johnstone (MSc)<sup>a,\*</sup>, Jonathan J. Wyatt (MSc)<sup>b</sup>, Ann M. Henry (MD)<sup>a,c</sup>, Susan C. Short (MBBS, PhD)<sup>a,c</sup>, David Sebag-Montefiore (FRCR)<sup>a,c</sup>, Louise Murray (PhD)<sup>a,c</sup>, Charles G. Kelly (FRCR)<sup>b</sup>, Hazel M. McCallum (PhD)<sup>b</sup> and Richard Speight (PhD)<sup>c</sup>

<sup>a</sup> Leeds Institute of Cancer and Pathology, University of Leeds, U.K.

<sup>b</sup> The Northern Centre for Cancer Care, The Newcastle-upon-Tyne NHS Foundation Trust, Newcastle-upon-Tyne, U.K.

<sup>c</sup> Leeds Cancer Centre, Leeds Teaching Hospitals NHS Trust, Leeds, U.K.

\*Corresponding author

Ead: [umerj@leeds.ac.uk](mailto:umerj@leeds.ac.uk)

Contact address: Leeds Institute of Cancer and Pathology, St James's University Hospital, Beckett Street, Leeds, U.K., LS9 7TF

Contact telephone number: +441132068989

Conflict of interest statement:

Dr. reports grants and personal fees from Leeds Institute of Cancer and Pathology, UK, grants from The Sir John Fisher Foundation, UK, during the conduct of the study; grants from Institute of Physics and Engineering in Medicine, UK, grants from Charlie Bear for Cancer Care, Newcastle, UK, outside the submitted work; .

Acknowledgements

We gratefully acknowledge funding for this work received from The Sir John Fisher Foundation, the Leeds Institute of Cancer and Pathology (LICAP), the Institute of Physics and Engineering in Medicine (IPEM) and Charlie Bear for Cancer Care.

**Abstract**

MRI offers superior soft tissue contrast as compared to CT, which is conventionally used for radiotherapy treatment planning (RTP) and patient positioning verification, resulting in improved target definition. The two modalities are co-registered for RTP, however this introduces a systematic error. Implementing an MRI-only radiotherapy workflow would be advantageous as this error would be eliminated, the patient pathway simplified and patient dose reduced. Unlike CT, in MRI there is no direct relationship between signal intensity and electron density, however various methodologies for MRI-only RTP have been reported. A systematic review of these methods was undertaken.

The PRISMA guidelines(1) were followed. Embase and Medline databases were searched (1996-03/2017) for studies which generated synthetic CTs (sCT)s for MRI-only radiotherapy. 61 articles met the inclusion criteria.

This review showed that MRI-only RTP techniques could be grouped into three categories: i]bulk density override ii]atlas-based and iii]voxel-based techniques, which all produce an sCT scan from MR image(s).

Bulk density override techniques either used a single homogeneous or multiple tissue override. The former produced large dosimetric errors (>2%) in some cases and the latter frequently required manual bone contouring. Atlas-based techniques used both single and multiple atlases and included methods incorporating pattern recognition techniques.

Clinically acceptable sCTs were reported, but atypical anatomy led to erroneous results in some cases. Voxel-based techniques included methods using routine and specialised MRI

sequences, namely ultra-short echo time imaging. High quality sCTs were produced, however use of multiple sequences led to long scanning times increasing the chances of patient movement. Using non-routine sequences would currently be problematic in most radiotherapy centres.

Atlas-based and voxel-based techniques were found to be the most clinically useful methods, with some studies reporting dosimetric differences of <1% between planning on the sCT and CT and <1mm deviations when using sCTs for positional verification.

## Introduction

Within the field of radiotherapy, there is increasing interest about the integration of magnetic resonance imaging (MRI) into the patient pathway(2). MRI is favoured for target and organ at risk (OAR) delineation over computed tomography (CT), which is conventionally used, due to its superior ability to differentiate soft tissue(3). This is of particular importance due to the increasing use of intensity modulated radiotherapy (IMRT) techniques, whereby areas of high dose can be sculpted conformally around the target, with a steep fall off in dose outside of this region(3).

Magnetic resonance (MR) images are fused by either rigid or deformable registration with CT scans which are required for dose calculations(2) for radiotherapy treatment planning (RTP). This, however, introduces a registration uncertainty, estimated to be in the range of 0.5-3.5 mm (1 standard deviation typically reported) for prostate and head patients(4-7), which is propagated throughout the treatment. The ability to use MRI alone would eliminate this error, as well as simplify the radiotherapy workflow and reduce the concomitant dose received by the patient, the latter being of particular benefit to paediatric patients requiring multiple scans during their radiotherapy treatment(8). The aim of MRI-only radiotherapy is to remove the planning CT scan from the workflow, and in its place use MR image(s) alone. MRI-only planning is increasingly appealing due to the development of MRI-guided treatment techniques, such as the MRI-linac(9). Here, online adaptive radiotherapy using MRI can be performed, taking advantage of the anatomical and functional information provided by the modality(10).

A challenge when using MRI alone for RTP is that MRI signal intensity does not uniquely relate to electron density, as is the case with CT(11). Instead, the MRI signal depends largely on the density of protons, as well as tissue relaxation properties(12). This means that MRI scans cannot be used directly for dose calculation during RTP, without some form of electron density correction. Additionally, in conventional MRI sequences there is an absence of signal from cortical bone. Therefore using images as references for positional verification, which is essential for image guided radiotherapy (IGRT), is an additional complication for MRI-only radiotherapy. Soft tissue matching is commonly used in some centres, and therefore IGRT using this technique would also need to be considered in an MRI-only radiotherapy workflow.

A number of techniques have been developed which attempt to introduce an MRI-only radiotherapy workflow. These methods produce a synthetic CT (sCT) (also commonly known as pseudo or substitute CT) from MR image(s) which can be used for RTP, and potentially positioning verification for IGRT. Examples of sCT images for prostate and head and neck patients can be seen in Figure 1.

Figure 1.

This article systematically reviews methods in the literature for the production of sCTs for the purposes of MRI-only RTP and use in an MRI-only radiotherapy workflow. This is a subject of increasing interest in radiotherapy, and therefore a review of sCT methods is warranted. A recently published review by Edmund and Nyholm (13) searched the Scopus database November 2015 for methods of sCT generation for MRI-only RTP and PET-MRI

attenuation correction. The authors summarised performance metric values of sCTs and discussed issues related to reporting. This paper brings the search up-to-date and aims to provide a summary of different methodologies and their potential clinical implementation, through a systematic search using the Medline and Embase databases.

There are other pertinent factors which need to be investigated before an MRI-only radiotherapy workflow can be introduced. These include the need to scan the patient in the radiotherapy treatment position, such as on an MRI-simulator, and the need for the correction and assessment of geometric distortions associated with MR images over a large field of view (FOV). Although these factors are essential for MRI-only planning, these issues are outside the scope of this review.

## **Method**

A systematic review of techniques was carried out using the preferred reporting items for systematic reviews and meta-analyses (PRISMA) guidelines(1). The Embase and Medline databases were searched from 1996 to March 2017 using defined criteria (Appendix 1). Papers were included which related to both MRI and radiotherapy. Additionally, the papers included either referred to MRI-only, sCTs, bulk density or synonyms for these terms in their title or abstract.

Following the database search, duplicated papers were removed and records screened for eligibility. Papers were included which related to the generation of sCTs for use in an MRI-only radiotherapy workflow. Papers focussing on PET-MRI attenuation correction methods

were not included. These methods use similar techniques to those in MRI-only RTP and have reported novel sCT generation methodologies producing results of high quality, however reviewing these papers systematically was outside the scope of this review. All papers identified during the search which related to PET-MRI were scanned to ensure that no information relating to the use of sCTs in an MRI-only radiotherapy workflow was excluded.

This study considered external beam radiotherapy only and therefore brachytherapy studies were excluded. Brachytherapy, as well as stereotactic radiosurgery (SRS) treatments can use an MRI-only radiotherapy workflow as standard practice. These assume the whole volume is water equivalent (WE). Papers were excluded which related to SRS technicalities and procedures, however papers reporting on novel sCT production for SRS patients were included. Papers discussing the use of MRI in radiotherapy, the integration of MRI into a radiotherapy workflow, cancer screening using MRI and staging and delineation of tumours using MRI were not included. MRI geometric distortion assessment, quality assurance (QA) of MRI-only radiotherapy workflows, fiducial marker assessment on MRI scans, and registration technique details are important aspects of implementing an MRI-only radiotherapy workflow. However performing a systematic review of these techniques was outside the scope of this review and therefore papers relating to these were excluded. Conference proceedings were not considered. These can contain valid methodologies, however the large number of relevant abstracts was not manageable in this review.

A citation search of the identified papers was performed. Each included study was assigned a methodology category. For each category a table of data was constructed. These tables provide a summary of the published techniques, including the key findings of each study and

other pertinent factors such as study size, anatomical site and, where appropriate, treatment technique. A discussion of the clinical feasibility of each methodology follows.

## Results

A flowchart of the systematic search process can be seen in Figure 2. The database search yielded 517 records. After duplicate removal, 393 records remained. Out of these, 44 papers matched the inclusion criteria and, from the citation search, an additional 17 papers were identified. Therefore 61 papers in total were included in this review.

Figure 2.

Reasons for exclusion of papers from the review can be seen in Table 1. The number of papers excluded for each reason is given.

Table 1.

The generation of sCTs for RTP could be grouped into three main methodology categories. These were bulk density assignments, atlas-based and voxel-based techniques, with the latter being subdivided into techniques using standard MRI sequences alone and those utilising ultra-short echo time (UTE) sequences. Studies have reported results using a range of metrics; issues related to the comparability of these will be discussed.

It should be noted that only the results of 56 studies are reported. This is due to 6 papers from the search, whilst being highly relevant to the generation sCTs for an MRI-only radiotherapy workflow, not directly testing novel sCT methodologies.

### **Bulk Density Override Techniques**

The simplest method to generate a dataset for dose calculation from an MR image is to apply a bulk density override to the entire patient volume, assigning it as WE electron density. This has been tested for brain sites(14-18), as well as for prostate and head and neck studies(19-22).

It can be seen from Table 2 that assuming a homogenous density across the volume can lead to dose discrepancies greater than 2% compared to planning heterogeneously on the CT. Korsholm et al., (23) has suggested that a 2% error in MRI dose calculation is clinically acceptable (assuming a 1% dose calculation error when using CT). In addition, with this technique, it is difficult to create reference images that could be used for patient positioning verification due to the lack of bone segmentation.

An alternative methodology is to separate the tissues in the MR image into different classes and assign every class an electron density or Hounsfield unit (HU) value. In most cases this involves two or three classifications; soft tissue and bone (and in some cases air). Improved dosimetric results have been reported using these techniques compared to using a homogeneous density override, namely for prostate, brain and head and neck sites(21-31).

Whilst most studies undertook segmentation of structures on the MRI, others(23, 24)

contoured the bone on the CT and then transferred the structures to the MRI before overriding densities. In an MRI-only radiotherapy workflow, this would not be possible. These studies were included in this review however, as the results are useful for assessing bulk density techniques for MRI-only planning. The overrides applied in the literature are summarised in Figure 3.

Figure 3.

The dosimetric results from these studies suggest that this technique has the potential to be used clinically, with dose differences of less than 2% typically reported when bone is segmented (Table 2). The appearance of cortical bone in conventional MR images however limits its advantages. Cortical bone has a very short T2\* relaxation time(2) and therefore in conventional MRI it is represented as a signal void. This makes it difficult to distinguish bone from air and has led many studies to resort to manual bone contouring. This is time-consuming and not practical for routine clinical use. In addition, artefacts such as those associated with dental implants can make segmentation in the head more difficult.

Stanescu et al., (31) attempted a semi-automatic method of bone segmentation in the head. Here, a point was placed close to the structure which required segmentation. Thresholding was then used to segment the structure. The authors noted that manual adjustment afterwards was required in some cases, particularly towards the lower section of the skull. Stanescu et al., (30) used an atlas-based segmentation method to separate the bone, prior to bulk density override. Again manual adjustment was used if necessary. Methods such as

these could mean that bulk density techniques are more useful in a clinical workflow in the future, although manual adjustment of contours would not be desirable.

There is debate in the literature over the most appropriate bone density assignment to use (Table 2). Densities assigned range from 1.19-2.10 gcm<sup>-3</sup>. Hoogcarspel et al., (32) stated that dose errors have arisen due to assigning a single bone density rather than separating the bone into individual components.

Varying degrees of dose accuracy for bulk density methods have been reported. This can in part be explained by the use of a different number of tissue classifications as well through assigning different bone density values.

Although most studies do not state the planning algorithms used for dose calculations, earlier studies are likely to use simpler models. Therefore it is likely that there is more uncertainty in these studies in terms of accurately modelling areas of inhomogeneity, particularly low density changes, as well as photon and electron scattering. This should be taken into account when assessing dosimetric differences.

By segmenting bone and assigning bulk densities, reference images for patient positioning can be created. Digitally reconstructed radiographs (DRR)s created using MRI with bulk density overrides have been compared to CT-derived DRRs for prostate and brain patients(15, 18-20, 33, 34). Doemer et al., (25) compared cone-beam computed tomography (CBCT)-to-MRI with CBCT-to-CT agreement for prostate patients. Differences in shift position maximal in the anterior-posterior (AP) direction of 0.15±0.25 cm were reported. The authors

postulated the reason disagreement was greatest in this direction was due to bowel preparation issues during MRI scanning.

In the following sections other methods of sCT generation are discussed. Some studies referenced compare the results for generated sCTs to bulk density techniques. Where this is the case, the bulk density results are listed in the relevant table.

Table 2.

### **Atlas-Based Techniques**

Atlas-based techniques typically use a single, standard MRI sequence in order to produce an sCT(35). This ensures that scanning time is kept to a minimum, reducing the chances of patient movement(35). It also means that the scanning protocol is straightforward to implement in a clinical environment. The process for sCT production can be fully automated and reference images for positioning verification can be produced as well as automatic contouring of OARs. Sjolund et al., (36) remarked how atlas-based techniques are relatively robust to image artefacts due to their reliance on prior training information.

The simplest atlas techniques use a single or average atlas, for example as developed by Dowling et al., (37) for prostate planning. With an average atlas technique, pairs of MRI and CT scans from a database of patients are co-registered. An average MRI atlas is then created, potentially with a matching set of organ contours. By determining the deformations which need to be applied to each MRI scan in the database to reach the average atlas, an

average CT atlas can be created by applying the same deformations to the corresponding registered CTs and finding the average of these. In order to create an sCT for an incoming MR image, the average MRI atlas is registered to the incoming MRI scan. These deformations are then applied to the average CT atlas resulting in a corresponding sCT. The organ contours can be propagated similarly.

Dowling et al., (37) validated their method through a 'leave-one-out' approach, which is commonly used in sCT evaluation (results in Table 3). Here the training atlas is determined using all patients except one. The scan of this excluded patient is used as an input in order to test the model. Differences in dose were found to be largely attributable to changes in external patient contour between MRI and CT scanning. Additional work by the group confirmed no significant difference in HU values for the main OARs between sCTs and CTs(38).

Demol et al., (4) used a single atlas as a baseline for brain MRI-only radiotherapy. Here, the co-registered MRI and CT of one patient is used rather than an average atlas. The authors reported significant dosimetric errors using this method. Additionally, it was found that for a test patient where a large section of skull had been removed, the sCT was assigned as bone in this area.

Several groups have reported improved quality sCTs when multiple atlases, combined with local patch-based pattern recognition methods, are used (Figure 4). By combining an atlas technique with these methods, the effect of uncertainty in image registration is reduced(39).

Figure 4.

Uh et al., (39) used a multi-atlas method for sCT production. Here, pairs of CT and MRI scans of brain patients were rigidly co-registered. When a new patient MRI was input, all MRI atlases were deformed to match the incoming image and these deformations were subsequently applied to the corresponding atlas CTs. The final sCT was calculated by combining the deformed CT atlases using a pattern recognition approach. Here, the intensity of each voxel in the sCT was a weighted average of voxel intensities from the deformed atlas CTs. The voxel in the same location in the atlas, as well as a defined number of neighbouring voxels (a patch), contributed to the prediction. For each voxel, the weighting of each atlas's contribution to the final sCT was determined by assessing the similarity of the patch between the MRI atlas and the incoming MR image. The smoothing of patient-specific anatomy was less pronounced with this weighted atlas technique compared to taking the average of the atlases.

Sjolund et al., (36) used multiple atlases to produce sCTs in the head. The collection of deformed CTs was iteratively registered to their joint voxel-wise mean. It was found however that using the voxel-wise median of the deformed CT dataset gave superior results.

Andreasen et al., (6) used a patch-based regression model for generation of brain sCTs using a multi-atlas approach based on affine registrations. Corresponding MRI patches and CT target values were extracted. A database of these was created for every patch location for every patient. For a patch in the test patient MRI, the CT number was assigned by

performing an intensity-based nearest neighbour search of the patch database. A similarity measure was used to weight the contribution of the patches. Additionally, the structural similarity measure(40), based on the mean and variance of the patches, was used in order to discard highly dissimilar patches and hence reduce the number of similarity comparisons required. The method was found to produce comparable quality sCTs to a multi-atlas method using non-linear registration.

This method was also tested on prostate patients(41). Before the patch search, atlases which were highly dissimilar to the patient scan were discarded. A significant reduction in the time needed to produce an sCT was achieved by implementing an approximate nearest-neighbour search of the patch database.

Dowling et al., (35) used a multi-atlas local weighting patch-based method to produce sCTs for prostate MRI-only planning. The authors added a 1 mm expansion to the body contour, which they proposed was necessary to compensate for missing signal from collagen in this area in the T2-weighted MR images.

Siversson et al., (42) used a multi-atlas method for the creation of sCTs for prostate MRI-only planning. The incoming MRI was auto-segmented into 5 structures; prostate, bladder, colon, bone and fat using a multi-template approach with machine learning. This was an automated segmentation algorithm which had been trained using MRI scans in the template database, along with their associated delineations. This was followed by a non-linear warping procedure whereby the template MRI atlases were deformed such that their segmented structures matched those of the incoming MR image. Linear deformations were

applied to the tissues, both within and between structures. A further constrained non-rigid registration was carried out in order to align fine-grained structures. A voxel-wise weighted median HU value of all deformed CT atlases was determined with the weighting based on the resemblance of the candidate sCT to the incoming MRI.

Edmund et al., (43) used a patch-based multi-atlas method in order to assess the feasibility of using the resulting sCTs for set-up verification of brain patients. Using the positional corrections for a CT-CBCT image match as a reference, the corrections for using the MRI and sCTs as reference images were assessed (results in Table 3).

As patch-based pattern recognition methods are typically used to weight the contribution of each atlas to the final sCT on a voxel-wise basis, the techniques are in part voxel-based. Although these methods fall naturally into the category of an atlas-based method, it is noteworthy that this overlap exists.

Table 3.

### **Voxel-Based Techniques**

An alternative method for the generation of sCTs is through voxel-based techniques. These can involve the use of standard or specialised sequences, such as UTE imaging. Some techniques use a mixture of the two. These methods create sCTs using MRI intensities from a number of sequences. With voxel-based techniques the need for accurate registration of an incoming MR image to an atlas is not necessary(35, 44) and no segmentation of images is

needed if statistical methods are used(45). These techniques are well-equipped to handle patients with atypical anatomy(35, 44) and have shown ability to separate bone from air(25, 45).

### **Voxel-Based Techniques: Standard MRI sequences**

A number of authors have developed voxel-based techniques using routine, clinical MRI sequences (results in Table 4).

A group (46) in Helsinki, Finland devised a method for sCT generation using T1/T2\*-weighted MR images for pelvic sites. MRI and CT images were registered using bony anatomy, and the MR images were normalised. For each patient 40 voxels within the cortical bone, trabecular bone and bone marrow were chosen at random. The corresponding HU values and MRI intensities of the identified points were used to generate a model. The authors also converted the MRI intensities of tissue outside bone(47). 1000 points were used to analyse the relationship between HU values and MRI intensities for soft tissue in the pelvis. The model divided MRI intensities into threshold-based sections for muscle, fat and urine, assigning bulk HU values. Between these tissue classes, the MRI intensities were converted into HU values using linear interpolation.

This study also developed a conversion model for brain patients using 700 points in bone and soft tissue. Separate models were applied for bone and soft tissue after autocontouring the bone. Post soft tissue assignment, bulk overrides were applied for fluid, white matter,

grey matter and the scalp. Between these tissue classes, linear interpolation was used to convert MRI intensities to HU values.

The same group (48) carried out a phantom study determining dose deviations behind bones in RTP when using this technique. Korhonen et al., (49) investigated bone outline errors on sCTs of prostate patients and the effect of these on dose calculation. Korhonen et al., (50) assessed prostate sCT-derived DRRs. Dose calculation accuracy of prostate sCTs created using this method for proton therapy have been investigated(51).

Kim et al., (52) used T1 and T2-weighted MR images, with co-registered CT images, to create sCTs for prostate patients. The bone was manually contoured. All remaining low intensity voxels on the MRI were assigned as air and a bulk HU override was used for these regions. A truth table was created in order to assign the remaining voxels a tissue class based on their MRI intensities. The signal intensities for these voxels were calculated using a weighted sum of all the MR images. sCTs generated using this method were compared to those created using bulk density override methods(53).

Yu et al., (54) used T1-weighted images to contour the airways (manually and through interpolation) for head and neck patients. Compact bone, spongy bone and soft tissue masks were generated using statistical characteristics of MRI intensities. The MRI intensities of the voxels were mapped to their respective CT number ranges for each tissue.

Table 4.

**Voxel-Based Techniques: Ultra-short echo time imaging**

A challenge of MRI-only planning is that cortical bone is difficult to differentiate from air using standard MRI sequences. This has led some authors to undertake time-consuming manual contouring of either bones or airways, which in certain cases relied on CT information. Dual UTE (dUTE) allows imaging of tissues with short  $T2^*$  relaxation times such as bone(55) allowing air and bone to be more easily segmented. Results of techniques using these sequences can be seen in Table 5. Some methods use UTE sequences alone, whilst others combine them with standard sequences. These techniques have so far only been clinically tested on brain patients.

Rank et al., (56) and Rank et al., (57) used a 2D turbo spin echo (TSE) sequence with proton density weighting, as well as a 3D dUTE sequence. The model parameters of a tissue classifier were determined by finding the voxel-wise correlation between the corresponding MRI and CT image sets for 2 brain patients. This classifier had as input MRI intensities from the image sets, as well as neighbourhood and co-ordinate information. For a test patient, the probability of a voxel belonging to a specific tissue class was determined using this model.

A group (58), (45) from Umea, Sweden used regression models in order to generate sCTs in the head region. dUTE was used, along with a T2-weighted 3D spin echo based, sampling perfection with application optimized contrasts using different flip angle evolution (SPACE) sequence. The additional use of the SPACE sequence enabled tissues with a long T1 value to be distinguished from air. Each of the MR images and the CT image were considered a

variable in the model, with the signal intensity of each voxel a sample of the variable. Two additional images for each MRI scan were derived using the mean and standard deviation of voxels in a 27-voxel neighbourhood. These were also input as model variables. Using Gaussian mean regression (GMR) the expected CT number of each voxel was determined using the variables in the model. The method takes spatial location into account in order to help discriminate between tissues located at different interfaces(59). Johansson et al., (60) attempted to use parallel imaging in order to reduce the imaging time needed for sCT generation. The authors evaluated different methods of parallel imaging.

Jonsson et al., (44) and Jonsson et al., (61) reported on the use of this method for intracranial targets, assessing DRRs. These authors reported that the greatest discrepancies were around the posterior nasal cavities. Yang et al., (62) compared UTE-MRI-derived DRRs to conventional DRRs for brain patients.

The Ann Arbor, Michigan group (63, 64) used statistical regression combined with spatial information in order to create brain sCTs. The authors used dUTE along with time-of-flight (TOF) angiography to image blood vessels. TSE Dixon (used to separate fat and water) and T1-weighted magnetisation prepared rapid gradient echo (MPRAGE) images were acquired(64). Air masks and vessel masks were created. Fuzzy c-means clustering with a spatial constraint was used to assign the remaining voxels a probability of belonging to each of 5 classes; fat, fluid, grey matter, white matter and bone. This allowed for a mixture of tissue types within one voxel. DRRs derived from this process were compared to CT-derived DRRs. The authors(64, 65) compared using standard UTE to using pointwise encoding time reduction with radial acquisition (PETRA) sequences.

PETRA is a type of UTE imaging. In standard UTE sequences, data is acquired during gradient ramp-up, which can lead to image artefacts, and a radial 'koosh-ball' trajectory is used to sample k-space(66). In PETRA, data acquisition begins after gradient ramp-up. In order to avoid a resulting gap in the centre of k-space, PETRA uses both radial and Cartesian sampling, the latter being used to fill the middle of k-space(66). PETRA is a clinically released sequence unlike standard UTE.

Zheng et al., (67) modified the method developed by Kim et al., (52) and applied it to brain studies. Here bone-enhanced images (created using inverted UTE and Dixon sequences) and air masks were input into the previous workflow, along with bone-enhanced fluid attenuated inversion recovery (FLAIR) and UTE imaging. MR images were segmented into 5 tissue classes: air, bone, fat, brain matter and cerebrospinal fluid using a Gaussian mixture model, and sCTs were generated using the voxel-based technique described previously(52). The same group tested the sCTs for use in IGRT(68).

Edmund et al., (69) undertook a review of the use of UTE in the creation of sCTs for brain patients. Three approaches were investigated; a threshold-based approach often performed for PET-MRI studies(69), a statistical regression approach, and a Bayesian method whereby for each voxel a probability of belonging to each Gaussian distribution i.e. tissue class is estimated. The voxels are assigned to the tissue class with the highest probability. The authors compared the methods to a bulk density override, setting the entire volume as WE.

There has been preclinical work investigating zero-echo time (ZTE) imaging(70) combined with other sequences, including UTE, which reported more accurate dose calculations compared to using UTE alone. This review has not identified any clinical investigations using this sequence.

Table 5.

### **Hybrid methods: Atlas and Voxel-based techniques**

Hybrid methods using elements of voxel-based and atlas-based techniques have been tested; examples are described below (results in Table 6).

Gudur et al., (71) used a voxel-wise technique with a Bayesian framework to create sCTs for brain patients. T1-weighted MR images were acquired and deformable image registration between an MRI atlas and the patient MRI was performed. The intensity of each voxel in the MRI scan and the knowledge of the geometry of the voxel compared to the reference anatomy were used to create two conditional probability distribution functions (PDF)s. The mean value of the PDFs for each voxel was used to determine its electron density. Bone and air could be differentiated on the T1 images due to the use of an atlas, and the impact of registration issues associated with an atlas were reduced by the additional use of intensity information. The main difficulty lay in the compromise between accurately representing detailed structures in the anatomy, whilst avoiding becoming over reliant on a single registration.

Demol et al., (4) compared a method using a single atlas, to a method combining atlas and intensity methods for brain patients. For each voxel, a search of the nearest 81 voxels was performed on the deformed MRI-atlas to identify voxels within 10% of the input intensity. The sCT value of the voxel was determined by averaging the CT atlas voxel values corresponding to those selected on the MRI atlas. This was found to give superior dosimetric results to using a single atlas.

Table 6.

## Discussion

A number of methodologies for generating sCT scans from MR images have been identified. Using WE homogenous overrides for the entire patient volume, whilst simple, gives unacceptable dosimetric results in some cases, for example when the beam passes through an air cavity in the head(15). It is not possible to use these images as references for patient positioning verification. Bulk density overrides can be used by separating out different tissue classes. Whilst this can give better dosimetric results, the need to segment bone, which is carried out manually in the majority of cases, makes this technique unappealing. It is possible that the use automatic segmentation techniques seen particularly in atlas-based(35) and some voxel-based techniques, such as Koivula et al., (51), would aid clinical implementation of bulk density overrides for some anatomical sites.

Atlas-based techniques are promising methods for MRI-only planning. They can be fully automated and use routine MRI sequences. The techniques can be carried out using a single

MRI sequence, ensuring scan time is kept to a minimum and reducing chances of patient movement. The techniques have been shown to produce results with good geometric and dosimetric accuracy for prostate and brain patients, particularly when multiple atlases are used, with dose deviations typically reported below 1%. It is feasible to produce accurate reference images for treatment verification, provided accurate registration between the atlas and incoming MR image is achieved. Additionally, the use of an atlas means that structures can be contoured automatically; a process which may result in a reduction of contour variability and improvement in clinical efficiency.

The drawbacks of atlas-based techniques largely lie in their ability to handle patients with atypical anatomy. Uh et al., (39) noticed larger errors in atlas deformation in cases where patients had a large tumour volume or surgical void. Use of a single atlas alone has been found to give unacceptable dose deviations(4). This is to be expected as a single atlas would be unable to handle atypical anatomy. The ability of the technique to generate an accurate sCT depends on the accuracy of the registration techniques used(39). This uncertainty in image registration, particularly for patients with atypical anatomy is a concern(44, 58). The quality of the MRI scans, which need to have a FOV large enough to encompass the entire body contour is also important. The need for multiple pairwise registration of images is computationally intensive(35). Johansson et al., (45) commented that atlas-based techniques, although considered robust in terms of average pixel intensity, are associated with geometrical uncertainties particularly outside of the head region.

It can be seen (Table 3) that a number of different atlas sizes have been employed.

Siversson et al., (42) suggested that there is limited benefit in increasing the atlas size

beyond 15 patients, however there does not seem to be a consensus in the literature.

Andreasen et al., (41) used an atlas pre-selection process, excluding highly dissimilar atlases before the patch search. These authors commented that the optimal number of atlases to select would vary depending on the similarity of the atlases to the incoming MRI(41). The optimal number of atlases may therefore be site specific. Further investigation into appropriate atlas numbers should be a focus of future work.

Voxel-based techniques have been shown to produce clinically acceptable geometric and dosimetric results. As with atlas methods, dose differences typically below 1% have been reported and the production of accurate reference images for IGRT has been shown to be feasible. These techniques have developed in recent years with the integration of UTE sequences, which have made automatic classification of cortical bone possible. These methods have the ability to better handle patients with atypical anatomy, due to not being reliant on an atlas. There is also no requirement for accurate registration of a new incoming MRI scan, although accurate registration is normally essential during the learning steps.

One drawback of voxel-based methods is the use of multiple sequences. These improve tissue classification but result in a longer scan time, increasing the potential for patient movement. Additionally, methods which rely solely on standard MRI sequences often require some manual contouring of bone or airways which would limit their use in the clinic.

A large proportion of voxel-based methods use non-standard sequences, such as UTE, in order to avoid manual segmentation of bone, however these are often not in routine clinical use, particularly in radiotherapy departments. UTE is associated with poor image quality (71,

72) and streak artefacts which become more severe outside of the head region meaning application to other sites may prove difficult(58). Areas such as the nasal septa continue to be problematic with voxel-based techniques. Improvements with the sequence may occur in the future.

It is noteworthy that across the techniques there is inconsistency in the criteria used to evaluate sCT quality and accuracy. This issue needs to be addressed in order to aid method comparisons. This could be achieved, for example, with the consistent reporting of average absolute deviations in HU values, differences in WE path lengths, calculating dose deviations and DVH parameters for volumes of interest in the patient, as well as the percentage change in monitor units for dosimetric studies when comparing sCTs to CTs.

The problem is apparent when comparing dosimetric agreement between sCTs and CTs between different studies. Many studies used gamma analysis(73) to evaluate similarity in dose distributions. However gamma analysis pass rate is dependent on a number of factors, including dose and distance-to-dose agreement criteria, the percentage dose below which points are excluded from the analysis, whether global or local gamma analysis has been carried out and whether it has been performed in 2 or 3 dimensions. This number of variables makes a direct comparison of different studies difficult. Andreasen et al., (41) suggested for example that for their gamma criteria (dose difference=1%, distance-to-dose agreement=1 mm, 10% dose threshold, 2D global gamma analysis) an average pass rate of 97% is acceptable clinically, however a value of 94% should be questioned. This however would only apply to this specific criteria.

Edmund and Nyholm (13) have discussed the difficulty in comparing methodologies even in the case where the same metrics and parameters are being reported. Patient selection and exclusion criteria, as well as the amount of data pre-processing will affect the reported results(13). Aspects such as treatment technique, beam quality and target and OAR variability will affect dosimetric results.

MAE is a common reporting metric for sCT generation. However, it should be used with caution as it is influenced by which voxels are included in the comparison. For example, if voxels outside the body are included this will likely result in MAE which suggests better results than in the body alone, the latter being the only area of clinical interest. Additionally, including bowel gas can skew results, leading to poorer results than in reality. Gas is not consistent between MRI and CT scanning, however it is unlikely to be present in the same anatomical region during treatment. Reporting techniques as in (4) whereby the error across the whole HU range is shown, would also be useful. In addition, there are differences in reporting dose deviations. It is important to report on maximum dose deviations, as well as the mean as this is highly relevant clinical information.

Edmund and Nyholm (13) further suggested the creation of a public database containing MRI and corresponding CT scans for different sites which could be used to test models, one advantage being that pre-processing differences would become apparent. Reporting the results of the methods compared to setting the MRI to WE tissue was also suggested(13).

Andreasen et al., (41) impressed the need to assess MAE values for each site separately. For example, brains sCTs generally have higher MAE values than prostate sCTs. This is due to the

differing amount of soft tissue relative to air and bone(41). Edmund and Nyholm (13) reported that for prostates, the typical MAE was around 40 HU, however for brains it was in the range of 80-200 HU. Our review support this, although it should be noted that some lower MAEs have recently been reported for brains; Koivula et al., (51) reported MAEs for the head which were similar to those reported for prostates.

Studies so far have been tested using relatively low patient numbers (typically less than 40). Some studies have tested their methods with very few patients (less than 10). Whilst this may show proof of principle, it is not enough to demonstrate clinical feasibility and it is highly unlikely that patients with atypical anatomy have been adequately tested. The need for clinical studies which test MRI-only planning techniques with a larger patient cohort is clear. A study involving over one hundred prostate patients is currently underway in Sweden(74), thus ensuring that a broad range of patient anatomies are tested.

The main sites tested are the prostate and brain, the latter a rigid site which saw initial development due to the need for attenuation correction in PET-MRI studies. Some other sites, such as head and neck have been extensively tested with bulk density override techniques (see Table 2). Application of MRI-only planning techniques to other anatomical sites is important and should be the focus of future research. At recent conferences some studies have reported on sCT generation outside of the pelvis and brain, for example in the thorax, abdomen, limbs(75), liver(76) and head and neck(77) and therefore it is likely that groups will publish on these in the near future.

Some centres have implemented MRI-only planning clinically for specific sites. The Helsinki, Finland group have treated 400 prostate patients with a dual regression approach and the Michigan group have treated brain patients using a probabilistic approach(13, 47, 63). Additionally, centres in New York, USA and Turku, Finland have recently started using a commercial solution developed by Philips for clinical sCT generation for prostate patients(78). An Australian group are running a trial involving 25 prostate patients, where planning is performed on the sCT(79).

The growing enthusiasm for MRI-only planning solutions is linked to the development of MRI-guided radiotherapy treatments. MRI-linacs are being developed worldwide, meaning that MRI-only planning would be necessary for full on-line plan adaption. The majority of clinics will not have access to an MRI-linac in the immediate future, however access to MRI-simulators and MRI diagnostic scanners is becoming more common for radiotherapy departments, meaning that many centres would be able to benefit from the advantages of MRI-only planning. The possibility of performing IGRT using either 2D or 3D image verification in an MRI-only radiotherapy workflow, without an MRI-linac, has been demonstrated in the reviewed literature. In order to use online adaptive planning, it would be desirable for sCT production time to be as short as possible. In the literature, where studies have reported sCT generation times, they have been in the range of 1-6 minutes for voxel-based techniques, a few minutes for average atlas studies and up to 80 mins for multiple atlas studies. Many studies do not report on the generation time; this should be included to assess the clinical suitability of the method.

QA in an MRI-only radiotherapy workflow has not been the focus of this review, however it is an essential requirement. Both geometric distortion analysis over the entire FOV, as well as end-to-end testing of the workflow, including IGRT testing should form part of the QA. As stated by Edmund and Nyholm (13), there is limited literature on tolerances regarding commissioning an MRI-only radiotherapy workflow and this should be discussed within the community in the near future.

### **Conclusion**

A systematic review has been performed to identify methods of sCT generation for MRI-only radiotherapy. Three main methods have been identified, with atlas-based and voxel-based techniques being the most clinically useful. Through this review, a number of non-vendor specific techniques have been identified, however interest in is growing in the radiotherapy community and commercial techniques are becoming available.

Due to the increasing appeal of MRI-only radiotherapy, studies with large patient cohorts should be undertaken in order to validate methods within an MRI-only radiotherapy workflow. Consensus regarding preferred metrics for reporting on the quality of sCTs should be reached.

1. Moher D, Liberati A, Tetzlaff J, Altman DG. Preferred reporting items for systematic reviews and meta-analyses: the PRISMA statement. *PLoS Med.* 2009;6(7):e1000097 10.1371/journal.pmed.1000097.
2. Nyholm T, Jonsson J. Counterpoint: Opportunities and Challenges of a Magnetic Resonance Imaging Only Radiotherapy Work Flow. *Seminars in Radiation Oncology.* 2014;24(3):175-80 10.1016/j.semradonc.2014.02.005.
3. Dirix P, Haustermans K, Vandecaveye V. The Value of Magnetic Resonance Imaging for Radiotherapy Planning. *Seminars in Radiation Oncology.* 2014;24(3):151-9 10.1016/j.semradonc.2014.02.003.
4. Demol B, Boydev C, Korhonen J, Reynaert N. Dosimetric characterization of MRI-only treatment planning for brain tumors in atlas-based pseudo-CT images generated from standard T1-weighted MR images. *Medical Physics.* 2016;43(12):6557 10.1118/1.4967480.
5. Nyholm T, Nyberg M, Karlsson MG, Karlsson M. Systematisation of spatial uncertainties for comparison between a MR and a CT-based radiotherapy workflow for prostate treatments. *Radiation Oncology.* 2009;4(1):1-9 10.1186/1748-717x-4-54.
6. Andreasen D, Van Leemput K, Hansen RH, Andersen JAL, Edmund JM. Patch-based generation of a pseudo CT from conventional MRI sequences for MRI-only radiotherapy of the brain. *Medical Physics.* 2015;42(4):1596-605 <http://dx.doi.org/10.1118/1.4914158>.
7. Ulin K, Urie MM, Cherlow JM. Results of a multi-institutional benchmark test for cranial CT/MR image registration. *International Journal of Radiation Oncology, Biology, Physics.* 2010;77(5):1584-9 10.1016/j.ijrobp.2009.10.017.
8. Schmidt M, A. , Payne G, S. . Radiotherapy planning using MRI. *Physics in medicine and biology.* 2015;60(22):R323 10.1088/0031-9155/60/22/R323.
9. Legendijk JJ, Raaymakers BW, Vulpen M. The magnetic resonance imaging-linac system. *Semin Radiat Oncol.* 2014;24 10.1016/j.semradonc.2014.02.009.
10. Kupelian P, Sonke J-J. Magnetic Resonance Guided Adaptive Radiotherapy: A Solution to the Future. *Seminars in Radiation Oncology.* 2014;24(3):227-32 10.1016/j.semradonc.2014.02.013.
11. Karlsson M, Karlsson MG, Nyholm T, Amies C, Zackrisson B. Dedicated magnetic resonance imaging in the radiotherapy clinic. *International Journal of Radiation Oncology, Biology, Physics.* 2009;74 10.1016/j.ijrobp.2009.01.065.
12. Sprawls P. *Magnetic Resonance Imaging: Principles, Methods, and Techniques: Medical Physics Publishing; 2000.*
13. Edmund JM, Nyholm T. A review of substitute CT generation for MRI-only radiation therapy. *Radiation Oncology.* 2017;12(1):28 10.1186/s13014-016-0747-y.
14. Schad LR, Blüml S, Hawighorst H, Wenz F, Lorenz WJ. Radiosurgical treatment planning of brain metastases based on a fast, three-dimensional MR imaging technique. *Magnetic Resonance Imaging.* 1994;12(5):811-9 [http://dx.doi.org/10.1016/0730-725X\(94\)92206-3](http://dx.doi.org/10.1016/0730-725X(94)92206-3).
15. Ramsey CR, Oliver AL. Magnetic resonance imaging based digitally reconstructed radiographs, virtual simulation, and three-dimensional treatment planning for brain neoplasms. *Medical Physics.* 1998;25(10):1928-34.
16. Prabhakar R, Julka PK, Ganesh T, Munshi A, Joshi RC, Rath GK. Feasibility of using MRI alone for 3D radiation treatment planning in brain tumors. *Jpn J Clin Oncol.* 2007;37 10.1093/jjco/hym050.
17. Wang C, Chao M, Lee L, Xing L. MRI-based treatment planning with electron density information mapped from CT images: a preliminary study. *Technology in Cancer Research & Treatment.* 2008;7(5):341-8.
18. Weber DC, Wang H, Albrecht S, Ozsahin M, Tkachuk E, Rouzaud M, et al. Open low-field magnetic resonance imaging for target definition, dose calculations and set-up verification during three-dimensional CRT for glioblastoma multiforme. *Clinical Oncology (Royal College of Radiologists).* 2008;20(2):157-67.

19. Chen L, Price RA, Wang L, Li J, Qin L, McNeeley S, et al. MRI-based treatment planning for radiotherapy: dosimetric verification for prostate IMRT. *International Journal of Radiation Oncology, Biology, Physics*. 2004;60 10.1016/j.ijrobp.2004.05.068.
20. Chen L, R. A. Price J, Nguyen TB, Wang L, Li JS, Qin L, et al. Dosimetric evaluation of MRI-based treatment planning for prostate cancer. *Physics in medicine and biology*. 2004;49(22):5157.
21. Eilertsen K, Nilsen Tor Arne Vestad L, Geier O, Skretting A. A simulation of MRI based dose calculations on the basis of radiotherapy planning CT images. *Acta Oncologica*. 2008;47(7):1294-302 10.1080/02841860802256426.
22. Karotki A, Mah K, Meijer G, Meltsner M. Comparison of bulk electron density and voxel-based electron density treatment planning. *Journal of Applied Clinical Medical Physics*. 2011;12(4):3522 <http://dx.doi.org/10.1120/jacmp.v12i4.3522>.
23. Korsholm ME, Waring LW, Edmund JM. A criterion for the reliable use of MRI-only radiotherapy. *Radiation Oncology*. 2014;9:16 <http://dx.doi.org/10.1186/1748-717X-9-16>.
24. Chin AL, Lin A, Anamalayil S, Teo BK. Feasibility and limitations of bulk density assignment in MRI for head and neck IMRT treatment planning. *Journal of Applied Clinical Medical Physics*. 2014;15(5):4851 10.1120/jacmp.v15i5.4851.
25. Doemer A, Chetty IJ, Glide-Hurst C, Nurushev T, Hearshen D, Pantelic M, et al. Evaluating organ delineation, dose calculation and daily localization in an open-MRI simulation workflow for prostate cancer patients. *Radiation Oncology*. 2015;10(1):1-9 10.1186/s13014-014-0309-0.
26. Jonsson JH, Karlsson MG, Karlsson M, Nyholm T. Treatment planning using MRI data: an analysis of the dose calculation accuracy for different treatment regions. *Radiation Oncology*. 2010;5:62 <http://dx.doi.org/10.1186/1748-717X-5-62>.
27. Kristensen BH, Laursen FJ, Logager V, Geertsen PF, Krarup-Hansen A. Dosimetric and geometric evaluation of an open low-field magnetic resonance simulator for radiotherapy treatment planning of brain tumours. *Radiotherapy & Oncology*. 2008;87(1):100-9 <http://dx.doi.org/10.1016/j.radonc.2008.01.014>.
28. Lambert J, Greer PB, Menk F, Patterson J, Parker J, Dahl K, et al. MRI-guided prostate radiation therapy planning: Investigation of dosimetric accuracy of MRI-based dose planning. *Radiotherapy & Oncology*. 2011;98(3):330-4 <http://dx.doi.org/10.1016/j.radonc.2011.01.012>.
29. Lee YK, Bollet M, Charles-Edwards G, Flower MA, Leach MO, McNair H, et al. Radiotherapy treatment planning of prostate cancer using magnetic resonance imaging alone. *Radiotherapy & Oncology*. 2003;66(2):203-16.
30. Stanescu T, Hans-Sonke J, Pervez N, Stavrev P, Fallone BG. A study on the magnetic resonance imaging (MRI)-based radiation treatment planning of intracranial lesions. *Physics in Medicine & Biology*. 2008;53(13):3579-93 10.1088/0031-9155/53/13/013.
31. Stanescu T, Hans-Sonke J, Stavrev P, Fallone G. 3T MR-based treatment planning for radiotherapy of brain lesions. *Radiology and Oncology*. 2006;40(2):125-32.
32. Hoogcarspel SJ, Van der Velden JM, Lagendijk JJ, van Vulpen M, Raaymakers BW. The feasibility of utilizing pseudo CT-data for online MRI based treatment plan adaptation for a stereotactic radiotherapy treatment of spinal bone metastases. *Physics in Medicine & Biology*. 2014;59(23):7383-91 10.1088/0031-9155/59/23/7383.
33. Chen L, Nguyen TB, Jones E, Chen Z, Luo W, Wang L, et al. Magnetic resonance-based treatment planning for prostate intensity-modulated radiotherapy: creation of digitally reconstructed radiographs. *International Journal of Radiation Oncology, Biology, Physics*. 2007;68(3):903-11.
34. Ramsey CR, Arwood D, Scaperoth D, Oliver AL. Clinical application of digitally-reconstructed radiographs generated from magnetic resonance imaging for intracranial lesions. *International Journal of Radiation Oncology\*Biophysics*. 1999;45(3):797-802 [http://dx.doi.org/10.1016/S0360-3016\(99\)00173-X](http://dx.doi.org/10.1016/S0360-3016(99)00173-X).
35. Dowling JA, Sun J, Pichler P, Rivest-Henault D, Ghose S, Richardson H, et al. Automatic Substitute Computed Tomography Generation and Contouring for Magnetic Resonance Imaging

- (MRI)-Alone External Beam Radiation Therapy From Standard MRI Sequences. *International Journal of Radiation Oncology, Biology, Physics*. 2015;93(5):1144-53 10.1016/j.ijrobp.2015.08.045.
36. Sjolund J, Forsberg D, Andersson M, Knutsson H. Generating patient specific pseudo-CT of the head from MR using atlas-based regression. *Physics in Medicine & Biology*. 2015;60(2):825-39 10.1088/0031-9155/60/2/825.
37. Dowling JA, Lambert J, Parker J, Salvado O, Fripp J, Capp A, et al. An atlas-based electron density mapping method for magnetic resonance imaging (MRI)-alone treatment planning and adaptive MRI-based prostate radiation therapy. *International Journal of Radiation Oncology, Biology, Physics*. 2012;83(1):e5-11 <http://dx.doi.org/10.1016/j.ijrobp.2011.11.056>.
38. Greer PB, Dowling JA, Lambert JA, Fripp J, Parker J, Denham JW, et al. A magnetic resonance imaging-based workflow for planning radiation therapy for prostate cancer. *Medical Journal of Australia*. 2011;194(4):S24-7.
39. Uh J, Merchant TE, Li Y, Li X, Hua C. MRI-based treatment planning with pseudo CT generated through atlas registration. *Medical Physics*. 2014;41(5):051711 <http://dx.doi.org/10.1118/1.4873315>.
40. Zhou W, Bovik AC, Sheikh HR, Simoncelli EP. Image quality assessment: from error visibility to structural similarity. *IEEE Transactions on Image Processing*. 2004;13(4):600-12 10.1109/TIP.2003.819861.
41. Andreasen D, Van Leemput K, Edmund JM. A patch-based pseudo-CT approach for MRI-only radiotherapy in the pelvis. *Medical Physics*. 2016;43(8):4742-52 10.1118/1.4958676.
42. Siversson C, Nordström F, Nilsson T, Nyholm T, Jonsson J, Gunnlaugsson A, et al. Technical Note: MRI only prostate radiotherapy planning using the statistical decomposition algorithm. *Medical Physics*. 2015;42(10):6090-7 <http://dx.doi.org/10.1118/1.4931417>.
43. Edmund JM, Andreasen D, Mahmood F, Van Leemput K. Cone beam computed tomography guided treatment delivery and planning verification for magnetic resonance imaging only radiotherapy of the brain. *Acta Oncologica*. 2015;54(9):1496-500 10.3109/0284186x.2015.1062546.
44. Jonsson JH, Johansson A, Soderstrom K, Asklund T, Nyholm T. Treatment planning of intracranial targets on MRI derived substitute CT data. *Radiotherapy & Oncology*. 2013;108(1):118-22 <http://dx.doi.org/10.1016/j.radonc.2013.04.028>.
45. Johansson A, Karlsson M, Yu J, Asklund T, Nyholm T. Voxel-wise uncertainty in CT substitute derived from MRI. *Medical Physics*. 2012;39(6):3283-90 <http://dx.doi.org/10.1118/1.4711807>.
46. Kapanen M, Tenhunen M. T1/T2 -weighted MRI provides clinically relevant pseudo-CT density data for the pelvic bones in MRI-only based radiotherapy treatment planning. *Acta Oncologica*. 2013;52(3):612-8 <http://dx.doi.org/10.3109/0284186X.2012.692883>.
47. Korhonen J, Kapanen M, Keyrilainen J, Seppala T, Tenhunen M. A dual model HU conversion from MRI intensity values within and outside of bone segment for MRI-based radiotherapy treatment planning of prostate cancer. *Medical Physics*. 2014;41(1):011704 <http://dx.doi.org/10.1118/1.4842575>.
48. Korhonen J, Kapanen M, Keyrilainen J, Seppala T, Tuomikoski L, Tenhunen M. Absorbed doses behind bones with MR image-based dose calculations for radiotherapy treatment planning. *Medical Physics*. 2013;40(1):011701 <http://dx.doi.org/10.1118/1.4769407>.
49. Korhonen J, Kapanen M, Keyrilainen J, Seppala T, Tuomikoski L, Tenhunen M. Influence of MRI-based bone outline definition errors on external radiotherapy dose calculation accuracy in heterogeneous pseudo-CT images of prostate cancer patients. *Acta Oncologica*. 2014;53(8):1100-6 10.3109/0284186x.2014.929737.
50. Korhonen J, Kapanen M, Sonke JJ, Wee L, Salli E, Keyrilainen J, et al. Feasibility of MRI-based reference images for image-guided radiotherapy of the pelvis with either cone-beam computed tomography or planar localization images. *Acta Oncologica*. 2015;54(6):889-95 10.3109/0284186x.2014.958197.

51. Koivula L, Wee L, Korhonen J. Feasibility of MRI-only treatment planning for proton therapy in brain and prostate cancers: Dose calculation accuracy in substitute CT images. *Medical Physics*. 2016;43(8):4634 [10.1118/1.4958677](https://doi.org/10.1118/1.4958677).
52. Kim J, Glide-Hurst C, Doemer A, Wen N, Movsas B, Chetty IJ. Implementation of a novel algorithm for generating synthetic CT images from magnetic resonance imaging data sets for prostate cancer radiation therapy. *International Journal of Radiation Oncology, Biology, Physics*. 2015;91(1):39-47 <http://dx.doi.org/10.1016/j.ijrobp.2014.09.015>.
53. Kim J, Garbarino K, Schultz L, Levin K, Movsas B, Siddiqui MS, et al. Dosimetric evaluation of synthetic CT relative to bulk density assignment-based magnetic resonance-only approaches for prostate radiotherapy. *Radiat Oncol*. 2015;10:239 [10.1186/s13014-015-0549-7](https://doi.org/10.1186/s13014-015-0549-7).
54. Yu H, Caldwell C, Balogh J, Mah K. Toward magnetic resonance-only simulation: segmentation of bone in MR for radiation therapy verification of the head. *International Journal of Radiation Oncology, Biology, Physics*. 2014;89(3):649-57 [10.1016/j.ijrobp.2014.03.028](https://doi.org/10.1016/j.ijrobp.2014.03.028).
55. Robson MD, Gatehouse PD, Bydder M, Bydder GM. Magnetic resonance: an introduction to ultrashort TE (UTE) imaging. *J Comput Assist Tomogr*. 2003;27(6):825-46.
56. Rank CM, Hunemohr N, Nagel AM, Rothke MC, Jakel O, Greilich S. MRI-based simulation of treatment plans for ion radiotherapy in the brain region. *Radiotherapy & Oncology*. 2013;109(3):414-8 <http://dx.doi.org/10.1016/j.radonc.2013.10.034>.
57. Rank CM, Tremmel C, Hunemohr N, Nagel AM, Jakel O, Greilich S. MRI-based treatment plan simulation and adaptation for ion radiotherapy using a classification-based approach. *Radiation Oncology*. 2013;8:51 <http://dx.doi.org/10.1186/1748-717X-8-51>.
58. Johansson A, Karlsson M, Nyholm T. CT substitute derived from MRI sequences with ultrashort echo time. *Medical Physics*. 2011;38(5):2708-14 <http://dx.doi.org/10.1118/1.3578928>.
59. Johansson A, Garpebring A, Karlsson M, Asklund T, Nyholm T. Improved quality of computed tomography substitute derived from magnetic resonance (MR) data by incorporation of spatial information--potential application for MR-only radiotherapy and attenuation correction in positron emission tomography. *Acta Oncologica*. 2013;52(7):1369-73 <http://dx.doi.org/10.3109/0284186X.2013.819119>.
60. Johansson A, Garpebring A, Asklund T, Nyholm T. CT substitutes derived from MR images reconstructed with parallel imaging. *Medical Physics*. 2014;41(8):082302 <http://dx.doi.org/10.1118/1.4886766>.
61. Jonsson JH, Akhtari MM, Karlsson MG, Johansson A, Asklund T, Nyholm T. Accuracy of inverse treatment planning on substitute CT images derived from MR data for brain lesions. *Radiation Oncology*. 2015;10(1):1-7 [10.1186/s13014-014-0308-1](https://doi.org/10.1186/s13014-014-0308-1).
62. Yang Y, Cao M, Kaprealian T, Sheng K, Gao Y, Han F, et al. Accuracy of UTE-MRI-based patient setup for brain cancer radiation therapy. *Medical Physics*. 2016;43(1):262-7 [10.1118/1.4938266](https://doi.org/10.1118/1.4938266).
63. Hsu SH, Cao Y, Huang K, Feng M, Balter JM. Investigation of a method for generating synthetic CT models from MRI scans of the head and neck for radiotherapy. *Physics in Medicine & Biology*. 2013;58 [10.1088/0031-9155/58/23/8419](https://doi.org/10.1088/0031-9155/58/23/8419).
64. Paradis E, Cao Y, Lawrence TS, Tsien C, Feng M, Vineberg K, et al. Assessing the Dosimetric Accuracy of Magnetic Resonance-Generated Synthetic CT Images for Focal Brain VMAT Radiation Therapy. *International Journal of Radiation Oncology, Biology, Physics*. 2015;93(5):1154-61 [10.1016/j.ijrobp.2015.08.049](https://doi.org/10.1016/j.ijrobp.2015.08.049).
65. Hsu SH, Cao Y, Lawrence TS, Tsien C, Feng M, Grodzki DM, et al. Quantitative characterizations of ultrashort echo (UTE) images for supporting air-bone separation in the head. *Physics in Medicine & Biology*. 2015;60(7):2869-80 [10.1088/0031-9155/60/7/2869](https://doi.org/10.1088/0031-9155/60/7/2869).
66. Grodzki DM, Jakob PM, Heismann B. Ultrashort echo time imaging using pointwise encoding time reduction with radial acquisition (PETRA). *Magn Reson Med*. 2012;67(2):510-8 [10.1002/mrm.23017](https://doi.org/10.1002/mrm.23017).
67. Zheng W, Kim JP, Kadbi M, Movsas B, Chetty IJ, Glide-Hurst CK. Magnetic Resonance-Based Automatic Air Segmentation for Generation of Synthetic Computed Tomography Scans in the Head

- Region. *International Journal of Radiation Oncology, Biology, Physics*. 2015;93(3):497-506  
10.1016/j.ijrobp.2015.07.001.
68. Price RG, Kim JP, Zheng W, Chetty IJ, Glide-Hurst C. Image Guided Radiation Therapy Using Synthetic Computed Tomography Images in Brain Cancer. *International Journal of Radiation Oncology, Biology, Physics*. 2016;95(4):1281-9 10.1016/j.ijrobp.2016.03.002.
69. Edmund JM, Kjer HM, Van Leemput K, Hansen RH, Andersen JA, Andreasen D. A voxel-based investigation for MRI-only radiotherapy of the brain using ultra short echo times. *Physics in Medicine & Biology*. 2014;59(23):7501-19 10.1088/0031-9155/59/23/7501.
70. Gutierrez S, Descamps B, Vanhove C. MRI-Only Based Radiotherapy Treatment Planning for the Rat Brain on a Small Animal Radiation Research Platform (SARRP). *PLoS One*. 2015;10(12):e0143821 10.1371/journal.pone.0143821.
71. Gudur MS, Hara W, Le QT, Wang L, Xing L, Li R. A unifying probabilistic Bayesian approach to derive electron density from MRI for radiation therapy treatment planning. *Physics in Medicine & Biology*. 2014;59(21):6595-606 10.1088/0031-9155/59/21/6595.
72. Keereman V, Fierens Y, Broux T, De Deene Y, Lonneux M, Vandenberghe S. MRI-based attenuation correction for PET/MRI using ultrashort echo time sequences. *J Nucl Med*. 2010;51(5):812-8 10.2967/jnumed.109.065425.
73. Low DA, Harms WB, Mutic S, Purdy JA. A technique for the quantitative evaluation of dose distributions. *Medical Physics*. 1998;25(5):656-61 10.1118/1.598248.
74. Persson E. Multi-center/multi-vendor validation of MRI only prostate treatment planning. 4th MR in RT symposium; Ann Arbor, Michigan, USA;2016.
75. Korhonen JK, K.; Seppala, T.; Kapanen, M.; Tenhunen, M. MRI-only based radiotherapy: heterogeneous pseudo-CT images in various body parts (poster). ESTRO 35; Turin, Italy; 2016.
76. Bredfeldt J. MRI only dose calculation for Liver SBRT. 4th MR in RT Symposium; Ann Arbor, Michigan, USA;2016.
77. Maspero M, Seevinck PR, Meijer GJ, Lagendijk JJW, Viergever MA, van den Berg CAT. SU-E-J-219: A Dixon Based Pseudo-CT Generation Method for MR-Only Radiotherapy Treatment Planning of the Pelvis and Head and Neck. *Medical Physics*. 2015;42(6):3316-  
doi:<http://dx.doi.org/10.1118/1.4924305>.
78. Perkins G. (Personal correspondance). Philips Electronics UK Ltd; 2017.
79. Greer PB. (Personal correspondance). Calvary Mater Newcastle, Newcastle, Australia;2017.

## Figure and Table Legends

Figure 1. Example sCT images for (left) a prostate patient (transaxial slice shown. Image adapted from Dowling et al., (35) with author's permission) and (right) a head and neck patient (sagittal slice shown). A blue cross-hair is visible. This sCT was generated from a T1-weighted MRI using the MriPlanner software (image provided by Spectronic Medical, Sweden).

Figure 2. Flowchart of the systematic review process in line with the PRISMA guidelines(1).

Figure 3. An illustration of bulk density override techniques using a brain site as an example. These can be (left to right) a WE override, bone density override or bone and air override. In the latter two cases the remaining tissue is assigned as WE.

Figure 4. Illustrating a multi-atlas technique for creating sCTs. A single sCT is created using weighting techniques based on pattern recognition in most cases.

Table 1. Reasons for exclusion of papers from the systematic review. The number of papers excluded for each reason is given.

Table 2. Summary of the findings of bulk density override techniques. Remaining tissue assigned as WE unless otherwise stated.

Table 3. Summary of the findings of atlas-based techniques.

Table 4. Summary of the findings of voxel-based techniques using standard MRI sequences.

Table 5. Summary of the findings of voxel-based techniques using UTE sequences.

Table 6. Summary of the findings of hybrid methods for sCT generation.

Table 1. Reasons for exclusion of papers from the review

<b>Reason for exclusion</b>	<b>Number of papers</b>
The general use of MRI in cancer treatment, not focused on MRI-only planning methods	141
Brachytherapy	37
The role of PET/ SPECT in cancer treatment	22
Stereotactic radiosurgery (SRS)/ radiosurgery technicalities	19
The integration of MRI into the radiotherapy pathway	16
PET-MRI	13
Target delineation with MRI	10
Staging with MRI	9
Not related to cancer	8
Screening with MRI	7
Chemotherapy	5
Not using MRI	4
Geometric distortions	4
Quality assurance	2
Fiducial marker assessment	3
Magnetic nanoparticles	2
The use of ultrasound in cancer treatment	1
Registration assessment	1
MRI sequence details	1
MRI-linac technicalities	1

Table 2. Summary of papers reporting on bulk density override techniques

	Number of patients	Anatomical site	Densities used	Treatment technique	Key findings	Positional verification
<b>(Schad et al., 1994)(14)</b>	10	Brain	WE	SRS	Dose difference <2%	N/A
<b>(Ramsey and Oliver, 1998)(15)</b>	Single phantom	Brain	WE	Conformal radiotherapy (CRT)	Dose difference <2% (beams passing through cranium), 2-4% (beams passing through air cavities)	DRRs (bones assigned using MRI intensities based on TE and TR) were structurally equivalent.
<b>(Ramsey et al., 1999)(34)</b>	16	Brain	Bones (low MRI values) assigned a pseudo density	DRR study only	DRR study only	DRR misalignments >3 mm could be identified.
<b>(Lee et al., 2003)(29)</b>	5	Prostate	1.WE 2.Bone assigned 320 HU	CRT	Dose difference 1. <5% high dose regions, 2. <2.7% planning treatment volume (PTV). Most high dose region <2%	N/A
<b>(Chen et al., 2004a)(19)</b>	15	Prostate	WE	Intensity modulated radiotherapy (IMRT)	Dose difference PTV <2%	DRRs created by manually contouring bone (applied density 2 gcm <sup>-3</sup> ). Accuracy <4mm.
<b>(Chen et al., 2004b)(20)</b>	15	Prostate	WE	CRT	Dose difference PTV <2.5%	DRRs created by manually contouring bone (applied density 2 gcm <sup>-3</sup> ). Accuracy < 3mm.
<b>(Stanescu et al., 2006)(31)</b>	4	Brain	Bone assigned 1.47 gcm <sup>-3</sup>	Not specified	Isodose distributions, dose volume histograms (DVH)s, tumour control probability (TCP) <1%	N/A

(Chen et al., 2007)(33)	20	Prostate	Bone assigned 2.0 gcm <sup>-3</sup>	DRR study only	DRR study only	DRR max difference 3mm
(Prabhakar et al., 2007)(16)	25	Brain	WE	CRT	Difference in DVH parameters statistically insignificant. Dose difference <2%	N/A
(Wang et al., 2008)(17)	6	Brain/ Intracranial	WE	IMRT	3-5% dose error	N/A
(Weber et al., 2008)(18)	10	Brain	WE	CRT	Planning brain tumours homogeneously is clinically acceptable	Set-up differences compared to CT-DRRs ranged from 1-4 mm
(Kristensen et al., 2008)(27)	11	Brain	1. WE. 2. Bone assigned 1.61 gcm <sup>-3</sup>	CRT	Clinical acceptable dose deviations if bone is segmented	N/A
(Stanescu et al., 2008)(30)	4	Brain	Bone assigned 1000 HU	IMRT	Difference in D <sub>max</sub> and D <sub>mean</sub> <1%. Difference in TCP <4%	Quality of DRRs not assessed
(Eilertsen et al., 2008)(21)	10	Prostate	1. WE 2. Bone assigned 1.30 gcm <sup>-3</sup> 3. Bone assigned 2.10gcm <sup>-3</sup>	CRT	Dose difference in target volume 1. <2.8% 2. <1.6%, 3. <9.7%	N/A
(Jonsson et al., 2010)(26)	40	Prostate, lung, head and neck, brain	Densities from ICRU 46 (cranium assigned 1.61 gcm <sup>-3</sup> , femoral bone assigned 1.33gcm <sup>-3</sup> )	CRT	Largest difference in MU 1.6%	N/A
(Karotki et al., 2011)(22)	10	Head and neck	1. WE 2. Bone assigned 1.50gcm <sup>-3</sup> , air assigned 0gcm <sup>-3</sup>	IMRT	1. 4-5% dose deviations reported 2.Target parameter dose difference <2%	N/A
(Lambert et al., 2011)(28)	39	Prostate	1. WE 2. Bone assigned 1.19 gcm <sup>-3</sup>	CRT	Dose difference 1. 2.6±0.9% 2. 1.3±0.8%	N/A

<b>(Korsholm et al., 2014)(23)</b>	57	Head and neck, prostate, vesica, pelvic	1. WE. 2. Bone assigned using ICRU 46 (age dependent) 3. In the head and neck. Bone assigned as in 2., air assigned 0 $\text{gcm}^{-3}$	Volumetric modulated arc therapy (VMAT)	2% dose difference in PTV coverage for 95% of patients fulfilled by all bulk density groups for DVH points, $D_{\text{median}}$ and $D_{2\%}$	N/A
<b>(Chin et al., 2014)(24)</b>	7	Head and neck	1. WE 2. Bone assigned 1.53 $\text{gcm}^{-3}$ 3. Bone assigned as in 2., air assigned 0 $\text{gcm}^{-3}$	IMRT	1. Overestimated target coverage by 15-30% 2. Reduced difference to <2% 3. Improved conformity at air-tissue interfaces	N/A
<b>(Doemer et al., 2015)(25)</b>	10	Prostate	Bone assigned 480 HU (based on average CT measurements)	IMRT	Dose difference <1%	CBCT-MRI cf CBCT-CT largest difference in AP direction (0.15±0.25 cm)

Table 3 Summary of papers reporting on atlas-based techniques

	Number of patients	Anatomical site	Atlas type (number used)	Treatment technique	Key findings	Positional verification
<b>(Greer et al., 2011)(38)</b>	39	Prostate	Single	Not a planning study	No significant difference in HU values for organs of interest Point dose difference <2%. No significant difference in Chi values or OAR HU values.	N/A
<b>(Dowling et al., 2012)(37)</b>	36	Prostate	Single	CRT	Mean dice similarity coefficient (DSC) 0.79, 0.70, 0.64, 0.63 for bone, prostate, bladder, rectum respectively. Multiple atlases outperformed single atlases. For these, dose difference $D_{95\%}$ and $V_{95\%}$ <2%. Pattern recognition had an equal performance of the mean. The root mean square difference was greater for WE override, and showed greater DVH differences. Mean error (ME) = $0.6 \pm 14.7$ HU. Mean absolute error (MAE) = $40.7 \pm 8.2$ HU. Mean DSC >0.80 for all organs. Change in MU = $0.3 \pm 0.8\%$ . 1.00 gamma pass rate (2%, 2mm)	DRRs could be generated
<b>(Uh et al., 2014)(39)</b>	14	Paediatric brain	1. Single random Arithmetic mean (6) 2. Pattern recognition (6) 3. Pattern recognition (6) 4. Pattern recognition (12)	CRT/ IMRT		N/A
<b>(Dowling et al., 2015)(35)</b>	39	Prostate	Multi-atlas (38) with local patch-based pattern recognition	IMRT		DRRs generated

(Siversson et al., 2015)(42)	10	Prostate	Multi-atlas (15) with local pattern recognition	VMAT	MAE = 36.5±4.1 HU. Average target dose difference =0.0±0.2%. Average gamma pass rate 99.9% (2%, 1mm)	N/A
(Sjolund et al., 2015)(36)	10	Head region	Multi-atlas (9) using iterative voxel-wise average	Not a planning study	Voxel-wise median performs better than voxel-wise mean	N/A
(Edmund et al., 2015)(43)	6	Brain	Multi-atlas (5) with local pattern recognition	Not a planning study	Average median absolute error 184±34 HU	Largest deviations of CT-CBCT were <1 mm and 1°
(Andreasen et al., 2015)(6)	5	Brain	Multi-atlas (3) patch based method	CRT	<0.5% dose difference in the target	Quality of DRRs not investigated
(Andreasen et al., 2016)(41)	10	Prostate	Multi-atlas 'leave-one-out' patch based method, with highly dissimilar atlases ignored	VMAT	Average MAE 54 HU. Average MAE WE path length 1.2 mm. Median deviation <0.4% relevant DVH points. Average gamma pass rate 97.0% (1%, 1 mm). Performed significantly better than WE override for the majority of metrics.	N/A

Table 4. Summary of papers reporting on voxel-based techniques (which use standard MRI sequences only)

	Number of patients	Anatomical site	Sequences used	Treatment technique	Key findings	Positional verification
<b>(Kapanen and Tenhunen, 2013)(46)</b>	10	Prostate	T1/T2* 3D gradient echo	CRT	Mean prediction error 135 HU. Maximal dose difference improved compared to WE and bone bulk density override.	Bone edge error <1 mm
<b>(Korhonen et al., 2013)(48)</b>	Phantom	Phantom	T1/T2* 3D gradient echo	6MV and 15MV CRT	Dose difference <1.3% (6MV) and <1.0% (15MV) behind bones (corresponding bone bulk density override values 2.7% and 2.0% respectively). Average local absolute difference 11 HU for soft tissue, 99 HU for bone. PTV dose difference <0.8%. 94% (IMRT) and 92% (VMAT) passed (1%, 1mm) gamma analysis. Significantly superior (dose, HU agreement) to WE override.	N/A
<b>(Korhonen et al., 2014a)(47)</b>	10	Prostate	T1/T2* 3D gradient echo	IMRT/ VMAT	1 mm bone segment error equivalent to 0.4% change in prostate dose level. Need <2mm bone segmentation error to achieve 2% dose consistency.	N/A
<b>(Korhonen et al., 2014b)(49)</b>	15	Prostate	T1/T2* 3D gradient echo	IMRT/ VMAT		N/A
<b>(Yu et al., 2014)(54)</b>	20	Brain (SRS)	T1	DRR study only	DRR study only	Maximum distance difference <1.88 mm. Mean geometric difference

						0.05±0.85 mm
<b>(Kim et al., 2015b)(52)</b>	9	Prostate	T1	IMRT	MAE 74.3±10.9 HU. Difference in mean target dose 0.63±0.34%. Gamma analysis pass rate 99.9±0.1% (2%, 2mm)	DSC for AP and lateral DRRs 0.90±0.04 and 0.92±0.05 respectively
<b>(Kim et al., 2015)(53)</b>	15	Prostate	T1/T2/Turbo field echo	IMRT/ VMAT	Better dose agreement for $D_{95\%}$ , $D_{99\%}$ , $D_{mean}$ (not statistically significant), significant improvements in the bladder cf bone bulk density and WE overrides. Gamma pass rate (1%,1mm) 97.2%, exceeded bulk overrides.	N/A
<b>(Korhonen et al., 2015)(50)</b>	5	Prostate	T1/ T2*	CBCT/ DRR study only	CBCT/ DRR study only	Standard deviation of difference <1.7 mm. Similarity metrics improved cf bulk sCT-DRRs.
<b>(Koivula et al., 2016)(51)</b>	20	10 Prostates and 10 brains	T1/ T2*	Intensity modulated proton therapy	MAE 34 HU (brain) and 42 HU (prostate). Maximum absolute dose difference in clinical target volume 1.4% (brain), 0.6% (prostate) (cf 1.8%, 8.9% in the brain and 1.2%, 3.6% in the prostate for bone bulk and WE override respectively). > 91%	N/A

passed gamma criteria  
(1%,1mm) (improved cf bulk  
density and WE).

ACCEPTED MANUSCRIPT

Table 5. Summary of papers reporting on voxel-based techniques (which use UTE sequences)

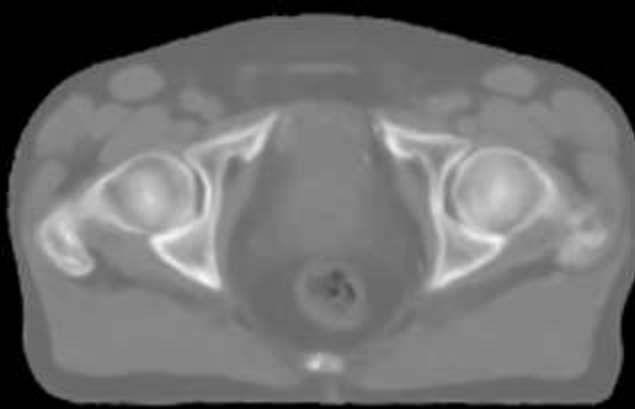
	Number of patients	Anatomical site	Sequences used	Treatment technique	Key findings	Positional verification
(Johansson et al., 2011)(58)	5	Brain	T2/ dUTE	N/A	MAE 137 HU. Accurately discriminated between bone and air.	N/A
(Johansson et al., 2012)(45)	14	Brain	T2/ dUTE	N/A	Mean absolute prediction deviation (MAPD) 140 HU. Largest error at air-soft tissue and bone-soft tissue interfaces.	N/A
(Johansson et al., 2013)(59)	9	Brain	4 UTE sequences	N/A	MAPD 130±18 HU. Accuracy improved by the inclusion of spatial information.	N/A
(Jonsson et al., 2013)(44)	5	Brain	T2/ dUTE	CRT	Dosimetrically identical to air and bone bulk density assigned plans. Improved cf WE.	sCT-DRRs sufficient for treatment set-up, but inferior quality around air cavities.
(Hsu et al., 2013)(63)	10	Brain	T1/ T2/ Dixon/ dUTE/ TOF	N/A	UTE showed significant improvement in discriminating bone and air. MAE <165 HU. Deviations at air cavities, bones and interfaces. PTV mean dose difference <2% (ions) and <0.2% (photons).	sCT-DRR comparable to CT-DRR. Bony edges of the skull were well visualised.
(Rank et al., 2013a)(56)	3	Brain	Proton density/ dUTE	Ions/ Photons	MAE <95 HU. Deviations at interfaces. PTV mean dose difference <3.1%	N/A
(Rank et al., 2013b)(57)	Phantom	Phantom	Proton density/ UTE/ T2/ MPRAGE	Ions	SPIRiT parallel imaging marginally improved sCT quality compared to gridding	N/A
(Johansson et al., 2014)(60)	23	Brain	dUTE (parallel imaging investigation)	N/A		N/A

(Edmund et al., 2014)(69)	5	Brain	2 dUTE	CRT	(however increased computational time) Statistical regression better geometrically cf Bayesian and threshold methods. All methods superior to WE. Statistical regression and threshold better dosimetrically than Bayesian. Mean difference $D_{min}$ and $D_{max} < 0.3\%$ . 100% of target voxels passed gamma analysis (1%, 1mm). 99.4-100% all voxels passed gamma analysis (3%, 3mm). DSC 0.8-0.9 for bones. UTE has significantly greater discriminating power in separating air and bone than PETRA	N/A
(Jonsson et al., 2015)(61)	5	Brain	2 dUTE	Not specified (optimised plans)	Mean dose parameter differences in target $< 1\%$ . No significant change in MU. OAR $D_{max}$ difference -2.2- (+1.9) Gy.	No appreciable differences for DRRs
(Hsu et al., 2015)(65)	12	Brain	UTE/ PETRA	N/A	MAE $147.5 \pm 8.3$ HU. Gamma analysis pass rate $99.4 \pm 0.04\%$ (1%, 1mm).	N/A
(Paradis et al., 2015)(64)	12	Brain	TSE Dixon/ MPRAGE/ TOF/ UTE	VMAT	For arced beams, the ZTE/ UTE (2 ms echo time) sequence combination was the most accurate: 0.7%	N/A
(Zheng et al., 2015)(67)	10	Brain	UTE/ Dixon/ T1 fast field echo (FFE)/ T2 TSE/ FLAIR	Not specified		
(Gutierrez et al., 2015)(70)	6	Pre-clinical	T1/ T2/ ZTE/ UTE	CRT/ arcs		

					deviation	
(Price et al., 2016)(68)	Phantom/ 12 patients	Brain	UTE/ Dixon/ T1 FFE/ T2 TSE/ FLAIR	Not a planning study	MAE 149.2±8.7 HU	sCT-DRRs within 1 mm of CT-DRRs
(Yang et al., 2016)(62)	7	Brain	UTE (2 echo times)	Not a planning study	Bone match <1 mm different of CT	Registration error between DRRs <1mm

Table 6. Summary of papers reporting on hybrid techniques

	<b>Number of patients</b>	<b>Anatomical site</b>	<b>Sequences used</b>	<b>Treatment technique</b>	<b>Key findings</b>	<b>Positional verification</b>
<b>(Gudur et al., 2014)(71)</b>	9	Brain	T1 Gradient echo	N/A	MAE 126 HU (cf 282 HU WE override). For 90% sensitivity in bone detection, 86% specificity.	N/A
<b>(Demol et al., 2016)(4)</b>	21	Intracranial	T1	SRS	Single atlas led to significant dose differences. Hybrid method performed better. Here, for 85% of the patients, mean dose difference to PTV<2%.	N/A



Identification

Records identified through  
database searching  
**517**

Records after duplicates removed  
**393**

Screening

Records screened  
**393**

Records excluded  
345  
(43 conference abstracts)

Eligibility

Full text articles  
assessed for eligibility  
**48**

Full text articles  
excluded  
4

Included

Studies included  
**44**

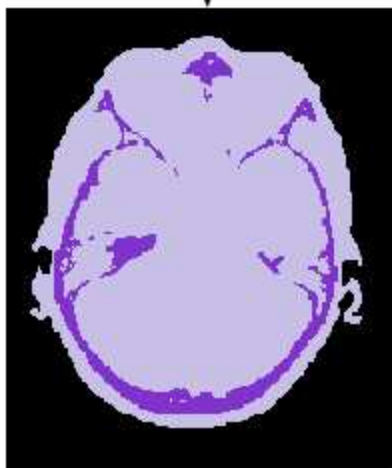
+

Records identified  
through citation search  
**17**

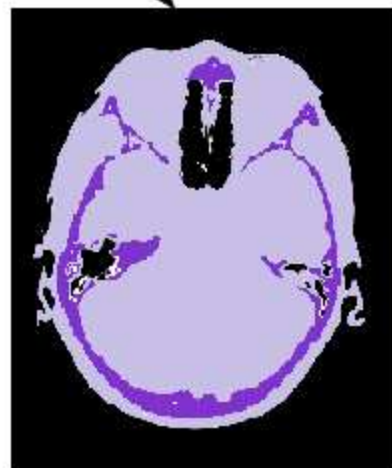
MR Image



Water  
equivalent  
override



Bone  
density  
override



Bone  
density  
and air  
override

